

# The Palermo *Swift*-BAT Hard X-ray Catalogue

## II. Results after 39 months of sky survey

G. Cusumano<sup>1</sup>, V. La Parola<sup>1</sup>, A. Segreto<sup>1</sup>, V. Mangano<sup>1</sup>, C. Ferrigno<sup>1,2,3</sup>, A. Maselli<sup>1</sup>, P. Romano<sup>1</sup>, T. Mineo<sup>1</sup>, B. Sbarufatti<sup>1</sup>, S. Campana<sup>4</sup>, G. Chincarini<sup>5,4</sup>, P. Giommi<sup>6</sup>, N. Masetti<sup>7</sup>, A. Moretti<sup>4</sup>, G. Tagliaferri<sup>4</sup>

<sup>1</sup> INAF, Istituto di Astrofisica Spaziale e Fisica Cosmica di Palermo, Via U. La Malfa 153, I-90146 Palermo, Italy

<sup>2</sup> Institut für Astronomie und Astrophysik Tübingen (IAAT)

<sup>3</sup> ISDC Data Centre for Astrophysics, Chemin d'Écogia 16, CH-1290 Versoix, Switzerland

<sup>4</sup> INAF – Osservatorio Astronomico di Brera, Via Bianchi 46, 23807 Merate, Italy

<sup>5</sup> Università degli studi di Milano-Bicocca, Dipartimento di Fisica, Piazza delle Scienze 3, I-20126 Milan, Italy

<sup>6</sup> ASI Science Data Center, via Galileo Galilei, 00044 Frascati, Italy

<sup>7</sup> INAF, Istituto di Astrofisica Spaziale e Fisica Cosmica di Bologna, via Gobetti 101, I-40129 Bologna, Italy

### ABSTRACT

**Aims.** We present the Palermo *Swift*-BAT hard X-ray catalogue obtained from the analysis of the the data relative to the first 39 months of the *Swift* mission.

**Methods.** We have developed a dedicated software to perform data reduction, mosaicking and source detection on the BAT survey data. We analyzed the BAT dataset in three energy bands (14–150 keV, 14–30 keV, 14–70 keV), obtaining a list of 962 detections above a significance threshold of 4.8 standard deviations. The identification of the source counterparts was pursued using three strategies: cross-correlation with published hard X-ray catalogues, analysis of field observations of soft X-ray instruments, cross-correlation with the SIMBAD databases.

**Results.** The survey covers 90% of the sky down to a flux limit of  $2.5 \times 10^{-11} \text{ erg cm}^{-2} \text{ s}^{-1}$  and 50% of the sky down to a flux limit of  $1.8 \times 10^{-11} \text{ erg cm}^{-2} \text{ s}^{-1}$  in the 14–150 keV band. We derived a catalogue of 754 identified sources, of which  $\sim 69\%$  are extragalactic,  $\sim 27\%$  are Galactic objects,  $\sim 4\%$  are already known X-ray or gamma ray emitters whose nature has not been determined yet. The integrated flux of the extragalactic sample is  $\sim 1\%$  of the Cosmic X-ray background in the 14–150 keV range.

**Key words.** X-rays: general - Catalogs - Surveys

## 1. Introduction

The study of Galactic and extragalactic sources at energies greater than 10 keV is fundamental to investigate non thermal emission processes and to study source populations that are not detectable in the soft X-ray energy band because their emission is strongly absorbed by a thick column of gas or dust. Another major aim of deep and sensitive surveys in the hard X-ray domain is to resolve the diffuse X-ray background (CXB) and identify which class of sources gives the larger contribution: while the CXB at energies lower than 10 keV has been almost entirely resolved (80–90%, Moretti et al. 2003; Worsley et al. 2005, 2006; Brandt & Hasinger 2005), only a  $\sim 1.5\%$  of the CXB at higher energies can be associated with resolved sources (Ajello et al. 2008b)

Up to now, the observation of the hard X-ray sky has not been performed with imaging grazing incidence telescopes because the reflectivity above 10 keV rapidly falls

down due to the steep decrease of the critical angle with energy. The first surveys in the hard X-ray domain were performed with detectors equipped with collimator-limited field of view: UHURU (2–20 keV; Forman et al. 1978) and HEAO1 (0.2 keV – 10 MeV; Wood et al. 1984). Later, sky images for energies greater than 10 keV have been produced using coded mask detectors (e.g. Fenimore & Cannon 1978; Skinner et al. 1987): in such detectors the entrance window of the telescope is partially masked and the “shadows” of the cosmic sources are projected onto a position-sensitive detector. Dedicated algorithms are then used to reconstruct the position and intensity of the sources in the field of view and, therefore, reproduce the image of the observed sky. In the last two decades space observatories equipped with this type of telescopes have surveyed the sky reporting detections of numerous sources emitting in the hard X-ray domain: Spacelab/XRT (Skinner et al. 1987), MIR/KVANT/TTM (Sunyaev et al. 1991), GRANAT/ART-P (Pavlinisky et al. 1992, 1994), GRANAT/SIGMA (Cordier et al. 1991; Sunyaev et al.

1991) and *BeppoSAX*/WFC (Jager et al. 1997). Today, the IBIS-ISGRI camera (Ubertini et al. 2003; Lebrun et al. 2003) on the INTEGRAL observatory (Winkler et al. 2003) with its field of view of  $8^\circ \times 8^\circ$  (fully coded) is carrying out a hard X-ray survey focussing mostly on the Galactic plane in the 20–150 keV energy band with sensitivity higher than previous observatories. The main results of this survey and the relevant source catalogues are reported in several papers (e.g. Bird et al. 2004, 2006, 2007; Bassani et al. 2006; Krivonos et al. 2007, 2005; Sazonov et al. 2007; Churazov et al. 2007).

The Burst Alert Telescope (BAT; Barthelmy et al. 2005) on board the *Swift* observatory (Gehrels et al. 2004), with its large field of view ( $100^\circ \times 60^\circ$  half coded) and large detector area (a factor of 2 greater than ISGRI) offers the opportunity for a large increase of the sample of objects that contribute to the luminosity of the sky in the hard X-rays allowing for a substantial improvement of our knowledge of the AGN and of the cosmic hard X-ray background. The first results on the BAT survey have been presented in Markwardt et al. (2005); Ajello et al. (2008a,b); Tueller et al. (2008). The latter presents a catalogue of sources detected in the first 9 months of the BAT survey data, identifying 154 extragalactic sources (129 at  $|b| > 15^\circ$ ).

In order to exploit the BAT survey archive, we developed the dedicated software *BATIMAGER* (Segreto et al. 2009), independent from the one developed by the Swift-BAT team<sup>1</sup>. In this paper we present the results obtained from the analysis of 39 months of BAT sky survey. The paper is organized as follows: in Sect. 2 we describe the BAT telescope; in Sect. 3 we describe the data set and screening criteria; in Sect. 4 we present a brief description of the code used for the analysis and illustrate our analysis strategy. In Sect. 5 we describe the survey properties. The catalogue construction and the results are reported in Sect. 6. The last Section summarizes our results. The spectral properties of our extragalactic sample will be discussed in a forthcoming paper (La Parola et al. 2009, in preparation).

The cosmology adopted in this work assumes  $H_0 = 70 \text{ km s}^{-1} \text{ Mpc}^{-1}$ ,  $k=0$ ,  $\Omega_m = 0.3$ , and  $\Lambda_0 = 0.7$ . Quoted errors are at  $1\sigma$  confidence level, unless otherwise specified.

## 2. The BAT telescope

The BAT, one of the three instruments on board the *Swift* observatory, is a coded aperture imaging camera consisting of a  $5200 \text{ cm}^2$  array of  $4 \times 4 \text{ mm}^2$  CdZnTe elements mounted on a plane 1 meter behind a  $2.7 \text{ m}^2$  coded aperture mask of  $5 \times 5 \text{ mm}^2$  elements distributed with a pseudo-random pattern. The telescope, operating in the 14–150 keV energy range with a large field of view (1.4 steradian half coded) and a point spread function (PSF) of 17 arcmin, is mainly devoted to the monitoring of a large fraction of the sky for the occurrence of Gamma Ray Bursts (GRBs). The BAT provides their position with the accuracy (1–4 arcmin) that is necessary to slew the spacecraft towards a GRB position and bring the burst location inside the field of view of the narrow field instruments in a couple of minutes. While waiting for new GRBs, it continuously col-

lects spectral and imaging information in survey mode, covering a fraction between 50% and 80% of the sky every day. The data are immediately made available to the scientific community through the public Swift data archive<sup>2</sup>.

## 3. Survey data set and screening criteria

We have analysed the first 39 months of the BAT survey data archive, from 2004 December to the end of 2008 February. The BAT survey data are in the form of Detector Plane Histograms (DPH). These are three dimensional arrays (two spatial dimensions, one spectral dimension) which collect count-rate data in (typically) 5-minutes time bins for 80 energy channels.

The data were retrieved from the *Swift* public archive and screened out from bad quality files, excluding those files where the spacecraft attitude was not stable (i.e., with a significant variation of the pointing coordinates). The resulting dataset was pre-analyzed (see Sect. 4), in order to produce preliminary Detector Plane Images (DPI, obtained integrating the DPH along the spectral dimension) from where the bright sources ( $S/N > 8$ ) and background were subtracted; very noisy DPHs, i.e. with a standard deviation significantly larger than the average value where subtracted. The list of bright sources detected in each DPH was used to identify and discard the files suffering from inaccurate position reconstruction. After cross-correlating the position of these sources with the ISGRI catalogue, the GRB positions and the newly discovered *Swift* sources documented in literature (Markwardt et al. 2005; Ajello et al. 2008a; Tueller et al. 2008), we discarded the files where:

- the bright sources in the BAT field of view are detected at more than 10 arcmin from their counterpart position (due to a star tracker loss of lock).
- the reconstructed image of at least one bright source has a strongly elongated shape (maybe due to an unrecognized slew).

After the screening based on these criteria, the usable archive has a total nominal exposure time of 72.7 Ms, corresponding to 91.2% of the total survey exposure time during the period under investigation.

## 4. Methodology

In order to perform a systematic and efficient search for new hard X-ray sources, we have developed the *BATIMAGER*, a dedicated software which produces an all-sky mosaic directly from a list of BAT data files. A complete and detailed description of the software and its performance is presented in Segreto et al. (2009). Here we only report the details of the procedure which are relevant to this work.

### 4.1. The code

The *BATIMAGER* integrates each single DPH in a selected energy range, producing the corresponding DPI. A preliminary

<sup>1</sup> <http://heasarc.gsfc.nasa.gov/docs/swift/analysis/>

<sup>2</sup> <http://heasarc.gsfc.nasa.gov/cgi-bin/W3Browse/swift.pl>

cleaning of the disabled and noisy pixels is performed, and the DPI is cross correlated with the mask pattern, in order to identify and subtract bright sources (with  $S/N > 8$ ). Then the background, modelled on a large scale from the analysis of the shadowgram residuals by performing a Principal Component Analysis (Kendall 1980), is subtracted. A further search for bad pixels is performed, obtaining the final map of all pixels to be excluded in the following steps. A further correction is applied to take into account differences in the detection efficiency of single detector pixels, through a time/energy dependent efficiency map, built stacking all the processed DPI and equalizing the average residual contribution for each pixel. The original DPI, corrected for the efficiency map and cleaned for the bad pixels, is processed again, with all the contributions from the background and the bright sources identified in the previous steps computed simultaneously, in order to correct for cross-contamination effects. These contributions are subtracted from the DPI, that is then converted into a sky image, using the Healpix projection (Górski et al. 2005). This projection provides an equal-area pixelization on a sphere and allows the generation of an all-sky map, avoiding the distortion introduced by other types of sky projections far from the projection center. This sky map is then corrected for the occultation of Sun, Earth and Moon. The sky maps produced from each DPI are added together, with the intensity in a given sky direction computed from the contribution from all the sky images, each inversely weighted for its variance in that direction. As described above, the bright sources and background were already subtracted from each single DPI; therefore this all-sky mosaic contains only the residual sky contribution. In order to correct for residual systematic effects (e.g. imperfect modelling of the source illumination pattern or of the background distribution), the all-sky  $S/N$  map is sampled on a scale significantly larger than the PSF: the local average  $S/N$  is subtracted and its measured variance used to normalize the local  $S/N$  distribution. Finally, we obtain a  $S/N$  map with zero average and unitary variance that can be used for a blind source detection.

#### 4.2. Detection strategy

We have created all-sky maps in three energy bands: 14–150 keV, 14–70 keV, 14–30 keV. The source detection in the all-sky map is performed by searching for local excesses in the significance map. The source position and its peak significance are then refined with a fit restricted within a region of a few pixels where the excess dominates over the noise distribution. Only detections with peak significance greater than 4.8 sigma are included in our list of detected sources. We found that this threshold represents the optimal value that maximizes the number of detectable sources, maintaining at the same time an acceptable number of spurious detections: taking into account the total number of pixels in the all sky map, the PSF and the Gaussian distribution of the noise, we expect 23 spurious detections above our threshold in each energy band, due to statistical fluctuations. Therefore, the total number of spurious detections will be between 23 and 69 (2.4% to 7.2% of the total number of our detections, see below), the best case occurring if each

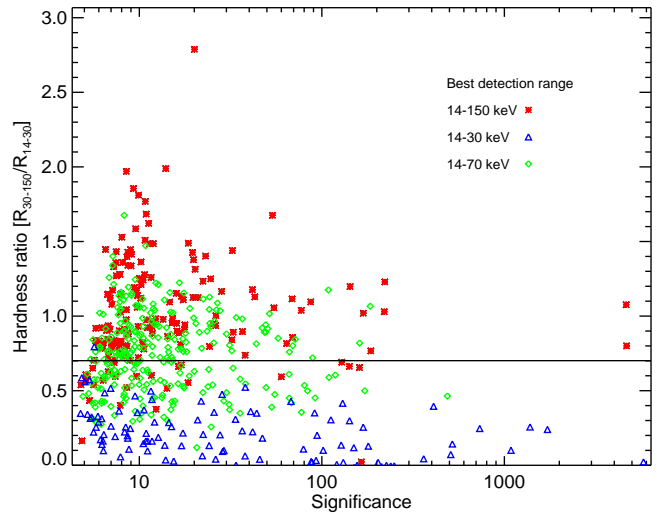


**Fig. 1.** Hardness ratio [defined as  $R(30-150)/R(14-30)$ ] of the sources detected with BATIMAGER as a function of the best detection significance. Different symbols refer to the energy range where each source was detected at the highest  $S/N$ . The solid line is the average hardness ratio value.

noise fluctuation above the threshold appears simultaneously in all three bands, the worst case occurring if each fluctuation appears only in one energy band. A few sources ( $\sim 5\%$ ) detected with a significance slightly lower than our threshold were included in the detection list because their  $S/N$  is significantly larger than the negative excess (in modulus) of the local noise distribution.

The resulting detection catalogues (one for each of the three energy bands) have been cross-correlated and merged in a single catalogue: when source candidates closer than 10 arcmin are present in the sky maps of different energy bands, they were reported in the merged catalogue as a single source candidate. We obtain a final number of 962 source candidates (detected in at least one of the three energy bands). We adopt as best source position the one corresponding to the energy range with the highest detection significance.

We have evaluated the hardness ratio of the detected sources as  $\text{Rate}(30-150 \text{ keV})/\text{Rate}(14-30 \text{ keV})$  (the hard rate is evaluated as the difference between the count rates in the 14–150 and in the 14–30 energy bands). In Figure 1 we plot the hardness ratio as a function of the significance for each detected source, showing the energy range where the detection has the highest significance. Repeating the detection process in three energy bands optimizes the  $S/N$  for each source, and this yields better values for the source position, whose uncertainty scales inversely with the significance. Moreover, a significant subsample of sources was detected in only one of the three energy bands (56 in the 14–150 keV energy band, 38 in the 14–30 keV energy band, 78 in the 14–70 keV energy band) demonstrating that searching in different energy bands maximizes the number of detectable sources.

Figure 2 shows that the distribution of the detected sources (orange squares) vs. Galactic latitude flattens for  $|b| > 5$ ,

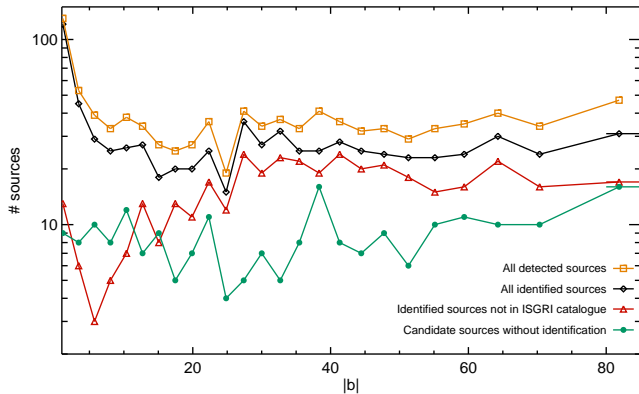


**Fig. 2.** Distribution of the detected sources vs. Galactic latitude. Each bin corresponds to a solid angle of  $\sim 0.50$  sr.

which we shall hereon consider our operational definition of the Galactic plane.

### 4.3. Identification strategy

The identification of the counterpart of the BAT detections was performed following three different strategies.

A. The position of each of the 962 detected excesses was cross-checked with the coordinates of the sources included in the INTEGRAL General Reference Catalogue<sup>3</sup> (v. 27), that contains 1652 X-ray emitters, and with the coordinates of the counterpart of the 48 new identifications of BAT sources already published (Markwardt et al. 2005; Tueller et al. 2008; Ajello et al. 2008a,b) and not included in the above catalogue. We adopted as counterpart a source within a radius  $R = 8.4$  arcmin from the BAT position (4 standard deviations error circle for a source detection at 4.8 standard deviations, Segreto et al. 2009). With this method we obtain 458 identifications, 295 with  $|b| > 5^\circ$ . The choice of the error radius is strategic to maximize the associations and keep the number of spurious associations to a negligible level. The number of spurious identifications due to chance spatial coincidence has been evaluated using the following expression:

$$N_{\text{sp}} = \frac{N \times A_R}{A} \times N_{\text{cat}} \quad (1)$$

where,  $A_R$  is the selected error circle area,  $A$  is the total sky area under investigation,  $N$  and  $N_{\text{cat}}$  are the number of BAT detections and of candidate counterparts in  $A$ . The above formula assumes both source distributions to be uniform over the sky. In order to take into account the higher density of sources on the Galactic plane we have divided the sky into two regions:  $|b| \leq 5^\circ$  (the Galactic plane, with  $N = 190$ ,  $N_{\text{cat}} = 651$ ) and  $|b| > 5^\circ$  ( $N = 772$ ,  $N_{\text{cat}} = 1049$ ). The number of expected spurious identifications is 2.1 within  $|b| < 5^\circ$  and 1.3 elsewhere. As the assumption of uniform distribution could be only a crude approximation, we have verified the evaluation of expected spurious associations with an alternative method:

we produced a set of 962 coordinate pairs by inverting the position of the detected excesses with respect to the Galactic reference system and cross-correlated these positions with the INTEGRAL General Reference Catalogue extended with the published BAT identifications. We obtained 3 spurious associations, in full agreement with the value obtained in Eq. 1.

B. We have searched for observations from *Swift*/XRT containing the remaining (504) unidentified excesses in their field. We found *Swift*/XRT observations for 186 BAT source candidates. Source detection inside these X-ray images was performed using XIMAGE (v4.4). When a source was detected inside a 6.3 arcmin error circle (99.7% confidence level for a source detection at 4.8 standard deviations, Segreto et al. 2009) we first checked for its hardness ratio in the 0.3–10 keV range (with 3 keV as a common boundary of the two ratio bands) and for its count rate above 3 keV. We identified a source as the counterpart of a BAT detection if at least one of the above conditions was satisfied: hardness ratio  $> 0.5$ , count rate above 3 keV  $> 5 \times 10^{-3} \text{ c s}^{-1}$ . In seven cases where two candidates, satisfying at least one of the threshold conditions, were found inside the BAT error circle, we chose as counterpart the closest source to the BAT position. With this method we identified 170 source counterparts. In order to evaluate the number of expected spurious identifications we collected a large sample of XRT observations of GRB fields, using only late follow-ups (where the GRB afterglow has faded) with the same exposure time distribution as the XRT pointings of the BAT sources. We searched for sources within a 6.3 arcmin error circle centered at the nominal pointing position in each of these fields, excluding any GRB residual afterglow, and satisfying at least one of the above threshold conditions. We detected 7 sources, therefore, the number of expected spurious identifications is consistent with the number of multiple XRT detections inside the BAT error circle. We also searched for field observations with other X-ray instruments (*XMM-Newton*, *Chandra*, *BeppoSAX*), finding 25 identifications, out of 30 pointings. Given the low number of available fields, the number of expected spurious identifications within this sample is irrelevant.

C. For the remaining unidentified sky map excesses (309) we searched for spatial coincidence inside an error circle of 4.2 arcmin radius (90% confidence level for a source detection at 4.8 standard deviations, Segreto et al. 2009) with sources included in the SIMBAD catalogues. The size of the search radius was fixed to 4.2 arcmin in order to have a negligible number of spurious identifications (see below). We restricted our search to the following SIMBAD object classes: Cataclysmic variable (CV), High mass X-ray binaries (HXB), Low mass X-ray binaries (LXB), Seyfert 1 (Sy1), Seyfert 2 (Sy2), Blazar and BL Lac (Bla, BLL), LINERs (LIN), for a total of 22425 objects in the SIMBAD database. This strategy allowed us to identify 92 detections, with only one source at low Galactic latitude ( $|b| < 5^\circ$ ). The number of expected spurious identifications was evaluated with the two methods described for the strategy A. According to Eq. 1 we expect 0.03 spurious identifications within  $|b| < 5^\circ$  (20 BAT detections and 391 Simbad sources in the classes of interest) and 2.7

<sup>3</sup> <http://isdc.unige.ch/?Data+catalogs>

elsewhere (289 BAT detections and 22034 Simbad sources); using the set of 309 coordinate pairs obtained inverting with respect to the Galactic center the positions of the sources in our sample we find 3 spurious associations, consistent with the first method. The cross correlation between unidentified sky excess and the SIMBAD catalogue of QSOs was treated separately because the coincidence error circle of 4.2 arcmin radius results in a high number of spurious associations (9 out of 17 associations). A radius of 2 arcmin allowed us to identify 9 sources as QSOs, and to optimize the ratio between the total number of associations and the expected number of spurious associations ( $\sim 2$ ).

In Fig. 3 we report the offsets of each BAT source with respect to its identified counterpart as a function of the detection significance (S/N). The offset vs. the detection significance can be modeled with a power-law plus a constant. The best fit equation we obtained is the following:

$$\text{Offset(arcmin)} = (9.1 \pm 1.6) \times (\text{S/N})^{-0.93 \pm 0.09} + (0.21 \pm 0.03) \quad (2)$$

The constant in Eq. 2 represents the systematic due to a residual boresight misalignment. At the detection threshold of 4.8 standard deviations the average offset is  $\sim 2.6$  arcmin.

Fig. 4 shows the distribution of the identified sources for each identification strategy as a function of the offset between the BAT position and the counterpart position. The peak of the distribution is at lower offset for strategy A because the sample of the sources identified with this strategy contains the brightest objects. The peak of the distribution relevant to strategy B is at a lower offset with respect to the distribution of strategy C because the XRT follow-up observations were performed on the more significant still unidentified source candidates.

All the identifications obtained with the three strategies (754) were merged in the final catalogue reported in Table 2 (see Section 6) where a flag indicates the identification method for each source. Figure 2 shows the distribution of all identified sources (black diamonds) as a function of the Galactic latitude.

A set of 208 detections could not be associated with a counterpart. These source candidates have detection significance between 4.8 and 14 standard deviations and flux in the 14–150 keV band between  $6.7 \times 10^{-12}$  and  $2.7 \times 10^{-11}$  erg cm $^{-2}$  s $^{-1}$ . 33 sources out of 208 are detected in all the three energy bands and 63 in two energy bands. The unidentified detections are distributed quite uniformly in the sky (Figure 2, green circles), with 190 sources out of 208 located above the Galactic plane ( $|b| > 5^\circ$ ).

## 5. Sky coverage and limiting flux

Figure 5 shows the sky coverage, defined as the fraction of the sky covered by the survey as a function of the detection limiting flux. The limiting flux for a given sky direction is calculated by multiplying the local image noise by a fixed detection threshold of 5 standard deviations. This threshold, higher than the one adopted for source detection (Sect. 4.2), was used to compare the BAT sky coverage with those produced with the INTEGRAL data survey. The large BAT field of

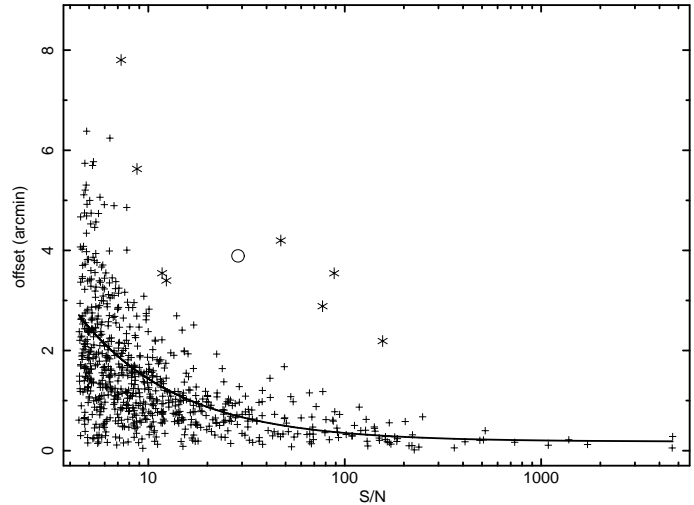


**Fig. 3.** Offset between the BAT position and the counterpart position as a function of the detection significance. A few values are far from the overall distribution: those marked with a star (sources number 535, 564, 565, 570, 571, 574, 584 and 586 in Table 2) are in crowded field and the reconstructed sky position suffers from the contamination of the PSF of the nearest sources; the one marked with a circle is an extended source (Coma Cluster). The solid line represents the fit to the data (excluding the few outliers) with a power law.

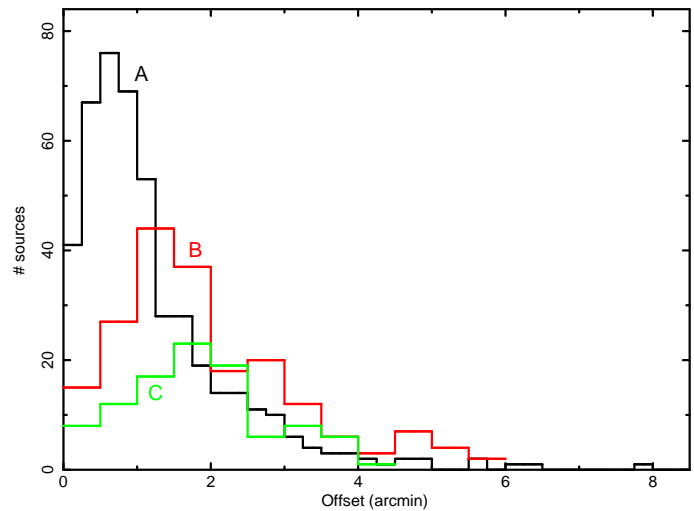


**Fig. 4.** Distribution of the identified sources for each identification strategy (Sect. 4.3) as a function of the offset between the BAT position and the counterpart position.

view, the large geometrical area together with the Swift pointing distribution, covering the sky randomly and uniformly according to the appearance of GRBs, has allowed the achievement of an unprecedented sensitive and quite uniform sky coverage. The 39 months BAT survey covers 90% of the sky down to a flux limit of  $2.5 \times 10^{-11}$  erg cm $^{-2}$  s $^{-1}$  (1.1 mCrab), and 50% of the sky down to  $1.8 \times 10^{-11}$  erg cm $^{-2}$  s $^{-1}$  (0.8 mCrab). In the same figure the BAT sky coverage is compared with that of INTEGRAL/ISGRI after 44 months of observation (Krivonos et al. 2007).

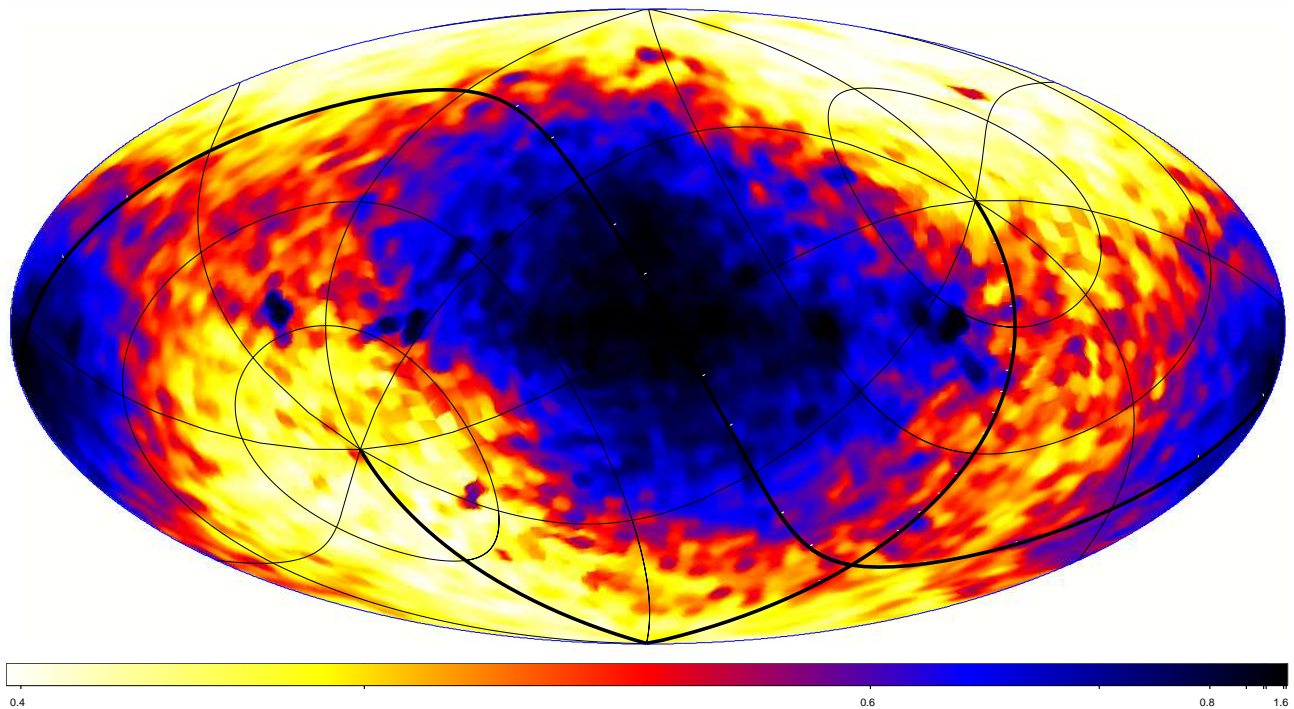


**Fig. 6.** Map of the limiting flux (in mCrab) of the 39-months BAT-survey data in the 14–150 keV band, projected in Galactic coordinates, with the ecliptic coordinates grid superimposed (the thick lines represents the ecliptic axes). The scale on the colorbar is in mCrab.

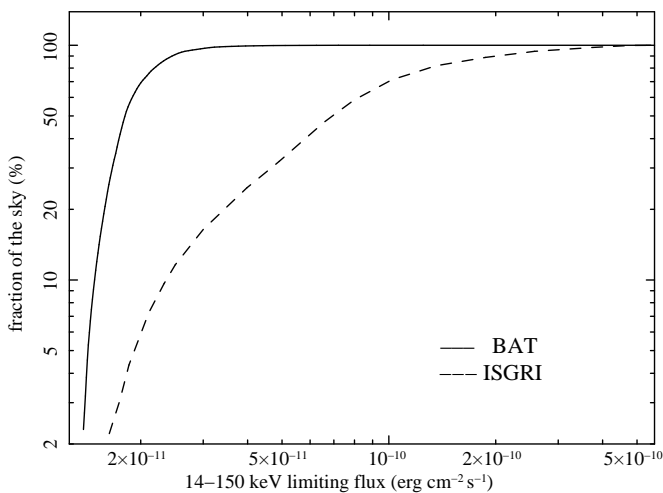


**Fig. 5.** Fraction of the sky covered by the *Swift*-BAT and INTEGRAL-ISGRI surveys vs. limiting flux.

Figure 6 shows the limiting flux map in galactic Aitoff projection, with the ecliptic coordinates grid superimposed. The minimum detection limiting flux is not fully uniform on the sky: the Galactic center and the ecliptic plane are characterized by a worse sensitivity due to high contamination from intense Galactic sources and to the observing constraints of the *Swift* spacecraft. The highest flux sensitivity is achieved near the ecliptic poles where a detection flux limit of about  $1.1 \times 10^{-11} \text{ erg cm}^{-2} \text{ s}^{-1}$  is reached ( $\sim 0.5$  mCrab).

## 6. The 39-months catalogue

The complete catalogue of the sources identified in the first 39 months of BAT survey data is reported in Table 2. The table contains the following information:

- Palermo BAT Catalogue (PBC) name of the source (column 2), built from the BAT coordinates with the precision of 0.1 arcmin on RA.
- Counterpart identification (column 3) and source type (column 4) coded according to the nomenclature used in SIMBAD.
- RA and Dec of the BAT source in decimal degrees (columns 5, 6).
- Error radius (column 7), offset with respect to the counterpart position (column 8) and significance (column 9), as obtained in the energy band with the highest significance (a flag in column 14 indicates the energy range with the maximum significance).
- Flux in the widest band of detection, averaged over the entire survey period (column 10). For most of the sources this is 14–150 keV. In the other cases a flag in column 14 indicates the appropriate band. In order to convert count rates into fluxes we derived a conversion factor for each of the three bands using the corresponding Crab count rate and the Crab spectrum used for BAT calibration purposes, as reported in the BAT calibration status report<sup>4</sup>.
- Hardness ratio defined as  $\text{Rate}[30\text{--}150 \text{ keV}]/\text{Rate}[14\text{--}30 \text{ keV}]$ , where the hard rate is evaluated as the difference be-

<sup>4</sup> [http://swift.gsfc.nasa.gov/docs/swift/analysis/bat\\_digest.html#calstatus](http://swift.gsfc.nasa.gov/docs/swift/analysis/bat_digest.html#calstatus)

Class	# of sources	% in the Catalog
LXB	76	10.1%
HXB	64	8.5%
Pulsars	10	1.3%
SN/SNR	5	0.7%
Cataclysmic variables	46	6.1%
Stars	5	0.7%
Molecular Cloud	1	0.1%
Galactic (total)	207	27.5%
Seyfert 1 galaxies	235	31.2%
Seyfert 2 galaxies	131	17.4%
LINERs	7	0.9%
QSO	14	1.8%
Blazars	71	9.4%
Galaxy clusters	18	2.4%
Normal galaxies	27	3.6%
Unclassified AGN	16	2.1%
Extragalactic (total)	519	68.8%
Other types	28	3.7%

**Table 1.** Classification of the known sources detected in the BAT survey. *Other types* includes all sources that have a catalogued counterpart but have not been classified yet.

tween the count rates in the 14–150 and in the 14–30 energy bands (column 11).

- Redshift of the extragalactic sources (column 12), from the SIMBAD database (or NED, for the few cases that were not reported in SIMBAD).
- Log of the rest frame luminosity in the 14–150 keV band for extragalactic objects (column 13), calculated using the luminosity distance for sources with redshift  $> 0.01$ , and using the distance reported in the Nearby Galaxies Catalogue (NBG, Tully 1988) or NED, for the few cases that were not reported in the NBG catalogue, for sources with redshift  $< 0.01$ .
- Flag column (column 14) with information on: energy band with the highest significance (A), energy band used for the calculation of the flux (B), flag for already known hard X-ray sources (C), position with respect to the Galactic plane ( $|b| < 5^\circ$ , D), strategy used for the identification (E, see Sect. 4.3)

### 6.1. Statistical properties of the catalogue

Table 1 details the distribution of the 754 sources in our catalogue among different object classes:  $\sim 69\%$  of the catalogue is composed of extragalactic objects,  $\sim 27\%$  are Galactic objects,  $\sim 4\%$  are already known X-ray or gamma ray emitters whose nature is still to be determined. Figure 7 shows the distribution of all the sources in our catalogue, colour-coded according to the object class, with the size of the symbol proportional to the 14–150 keV flux (for those sources not detected in the 14–150 keV band the flux in the widest band of detection has been extrapolated to the 14–150 keV range using the BAT Crab spectrum).

We have compared this distribution with the third ISGRI catalogue (Bird et al. 2007). The results are plotted in Figure 8.

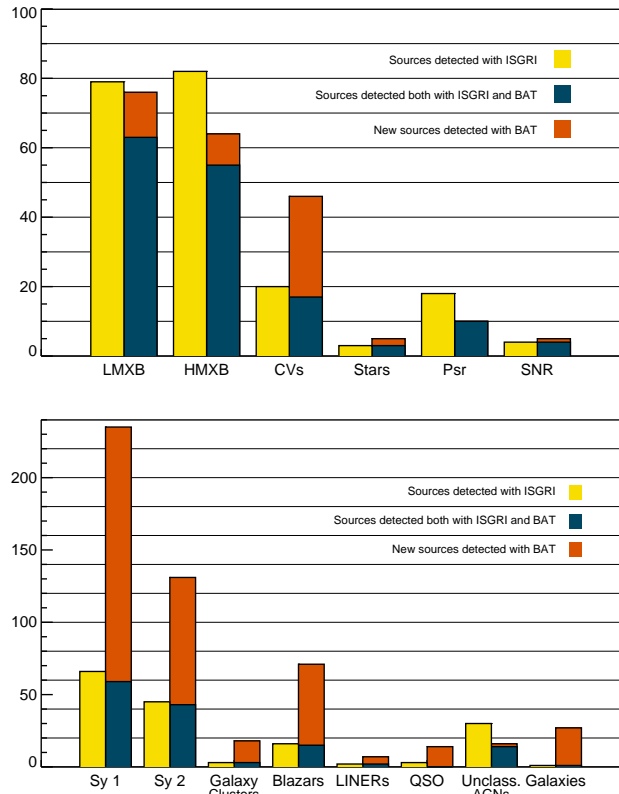


**Fig. 8.** Comparison between the sources in our catalogue and those reported in the third ISGRI catalogue (Bird et al. 2007). Top: Galactic sources. Bottom: Extragalactic sources.

We find a dramatic improvement in the detection of extragalactic objects, both in the nearby Universe (normal galaxies, LINERs) and at higher distances (Seyfert galaxies, QSO, clusters of galaxies). As expected from the sky coverage achieved by the BAT survey data (Figure 5), most of our identified sources have a flux below  $1 \times 10^{-10}$  erg s $^{-1}$  cm $^{-2}$  and are located outside the Galactic plane. We also detect many Galactic sources that are not included in the ISGRI catalogue, most of which are cataclysmic variables and X-ray binaries. This can be explained in part with the different pointing strategy of the two instruments. However, Figure 2 shows that, although most of our newly identified sources (red triangles) are above the Galactic plane, where the ISGRI exposure is low, we also detect a few sources on the Galactic plane most of which we identify as X-ray binaries (1E 1743.1–2852, GRO 1750–27, SAX J1810.8–2609 and XTE J1856+053). We have verified that their detections are due to a transient intense emission observed in the large FoV of BAT.

We detect emission from 18 clusters of galaxies. We verified that for 17 of them the spectral distribution in the 14–150 keV band is consistent with the tail of a thermal emission with  $kT \sim 10$  keV without evidence for the presence of a hard non-thermal emission. Only for Abell 2142 we find evidence for a power law component that could be ascribed to the AGN content of the cluster.

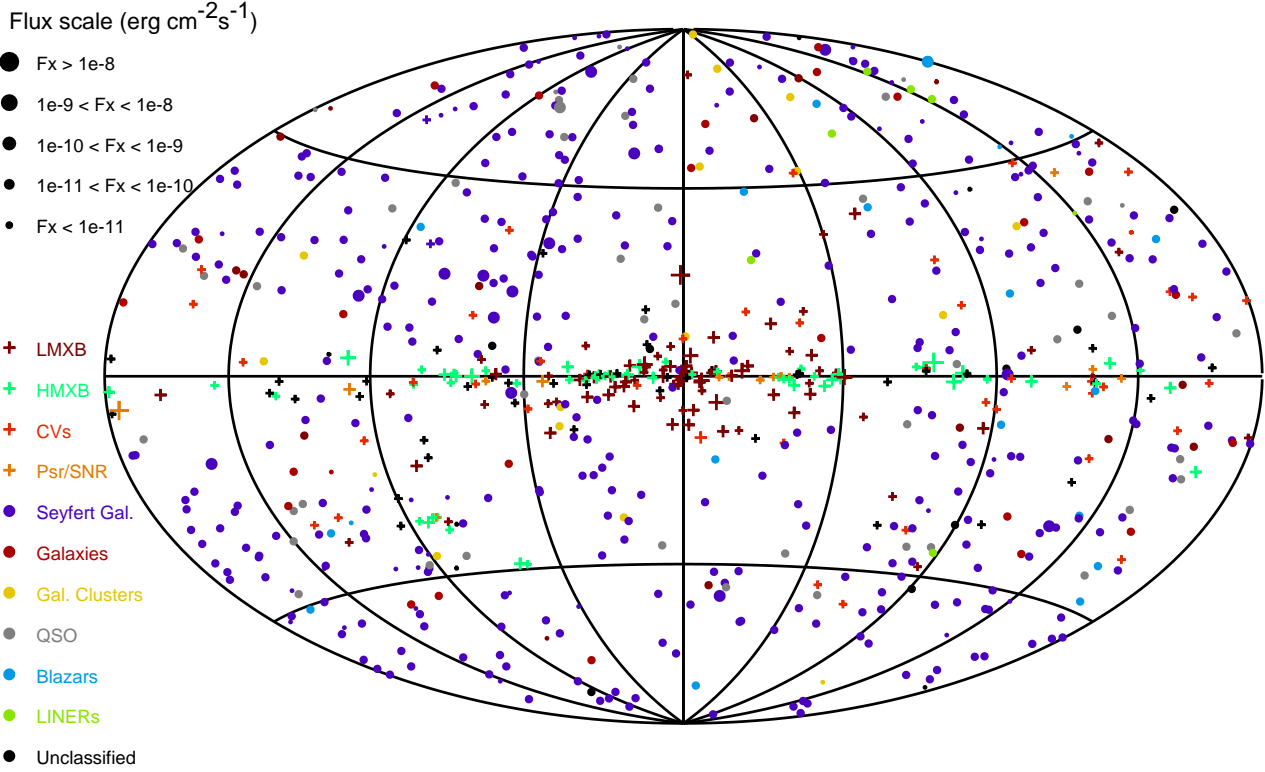


**Fig. 7.** Map of the sources we detect in the BAT survey data (Galactic coordinates). Different colors denote different object classes, as detailed in the legend. The size of the symbol is proportional to the source flux in the 14-150 keV band.

## 6.2. The extragalactic subsample

The catalogue contains 519 extragalactic objects. Figure 9 shows the distribution of the redshift within our sample for the main classes of extragalactic objects. Most of the emission-line AGNs are located at  $z < 0.1$ , but we also detected a few Seyfert 1 galaxies at larger redshift (up to  $\sim 0.29$ ). Seyfert 2 galaxies are detected up to  $z \sim 0.4$ . Blazars are detected up to  $z \sim 3.7$ , and QSOs are detected up to  $z \sim 2.4$ .

We verified the completeness of our sample of 366 emission line galaxies (i.e. the significance limit down to which we are including in the sample all objects above a given flux limit) using the  $V/V_{\text{Max}}$  test (Schmidt 1968; Huchra & Sargent 1973). This method was developed to test the evolution of complete samples of objects, but can be also used to test the completeness of non-evolving samples. For each source,  $V$  is the volume enclosed by the object distance, while  $V_{\text{Max}}$  is the volume corresponding to the maximum distance where the object could be still revealed in the survey (and thus depends on the limiting flux in the direction of the object). In case of no evolution the expected value of  $\langle V/V_{\text{Max}} \rangle$ , averaged over the entire sample, is 0.5. We assume the hypothesis of no evolution and uniform distribution in the local Universe. For each source in the sample, and for each significance level tested for completeness ( $\sigma_T$ ), we compute the quantity  $V/V_{\text{Max}}$  as  $[F/\sigma_T \Delta F]^{-3/2}$ , where  $F$  is the flux of the source and  $\Delta F$  its 1 standard deviation uncertainty.  $\langle V/V_{\text{Max}} \rangle$  is obtained averaging  $V/V_{\text{Max}}$  over the number  $N$  of all sources in the sample detected with a

significance higher than  $\sigma_T$ , and its error is  $1/12N$ . Figure 10 shows the results of this test: the distribution becomes constant at  $S/N \gtrsim 4.5\sigma$ , with a mean value of  $0.497 \pm 0.007$ , consistent with the expected value of 0.5. Thus we can confidently assume that our sample is complete down to our adopted significance threshold of  $4.8\sigma$ .

## 6.3. $\log(N) - \log(S)$ distribution

The  $\log(N) - \log(S)$  distribution was evaluated by summing the contribution of all the detected sources firmly identified with extragalactic objects (Table 2) and all the unidentified detections. We selected only sources with  $|b| > 5^\circ$ : Figure 2 (orange squares) shows that the detection distribution is uniform above this Galactic latitude limit. The cumulative distribution is weighted by the area in which these sources could have been detected. The following formula has been applied:

$$N(> S) = \sum_{S_i > S} \frac{1}{\Omega_i},$$

where  $N$  is the total number of detected sources with fluxes greater than  $S$ ,  $S_i$  is the flux of the  $i$ -th source and  $\Omega_i$  is the sky coverage associated to the flux  $S_i$  (Figure 5).

In order to avoid the presence of systematic errors in the determination of the  $\log(N) - \log(S)$  arising because of spurious source detections and to the large relative uncertainty on the sky coverage at the lower end of the flux scale, we limited the



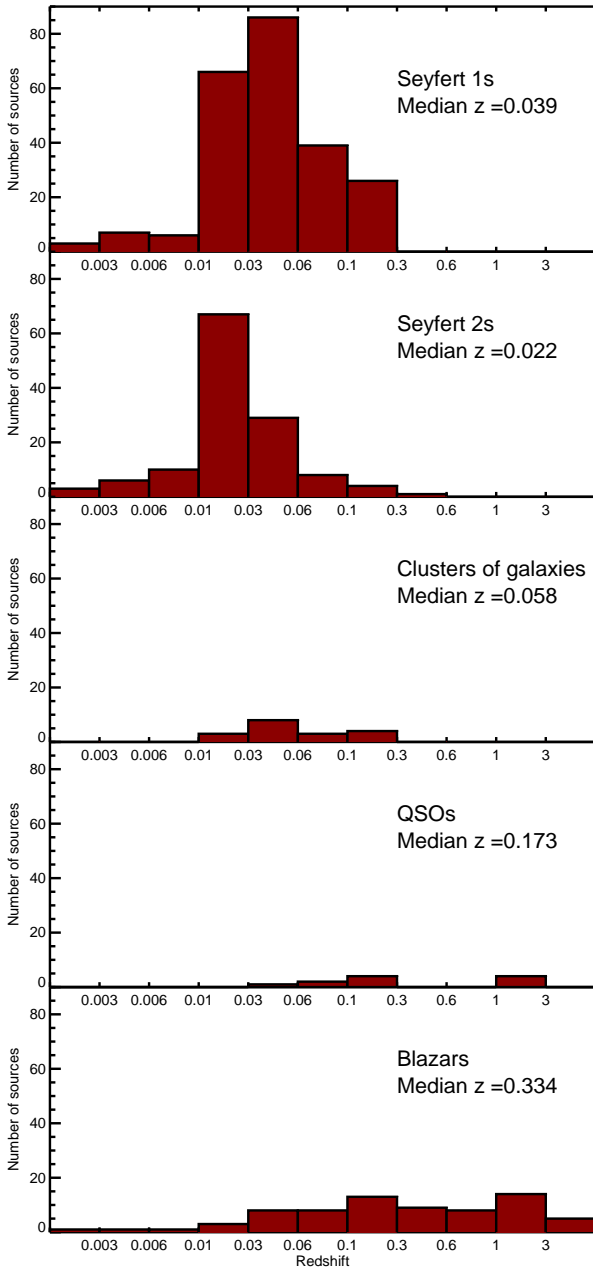


**Fig. 9.** Redshift distribution of the extragalactic sources in the BAT survey catalogue for different classes of extragalactic sources.

construction of the  $\log(N) - \log(S)$  to fluxes greater than  $\sim 1.5 \times 10^{-11} \text{ erg cm}^{-2} \text{ s}^{-1}$ . The resulting  $\log(N) - \log(S)$  distribution contains 330 sources (14 unidentified) and covers a flux range up to  $3 \times 10^{-10} \text{ erg s}^{-1} \text{ cm}^{-2}$ .

We applied a linear least-square fit to derive the slope of the  $\log(N) - \log(S)$  distribution assuming a power law in the form  $N(> S) = K \times (S/S_0)^{-\alpha}$ , where  $S_0$  is set to  $1 \times 10^{-11} \text{ erg cm}^{-2} \text{ s}^{-1}$ . The fit gives a value of  $\alpha = 1.56 \pm 0.06$  and a normalization of  $570 \pm 24$  sources with flux greater than  $10^{-11} \text{ erg cm}^{-2} \text{ s}^{-1}$ , corresponding to a density of  $(1.38 \pm 0.06) \times$

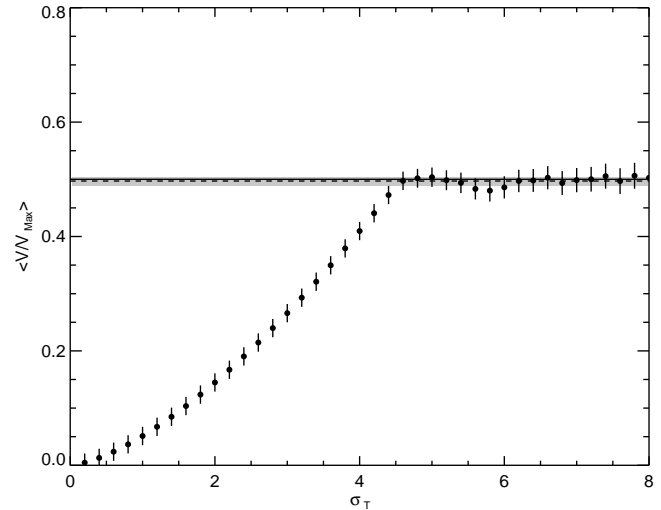


**Fig. 10.**  $\langle V/V_{\text{Max}} \rangle$  vs significance for our sample of extragalactic sources. The solid line is the expected value (0.5), the dashed line is the average value for  $S/N > 4.5\sigma$ , the shaded area covers the  $1\sigma$  error for the average value.

$10^{-2} \text{ deg}^{-2}$ . The single power-law model is found to give an acceptable description of the data ( $\chi^2 = 0.65$ ; 31 dof) with a slope consistent with an Euclidean distribution.

The presence of spurious detections in the sample of unidentified sources could introduce a systematic effect both in the slope and in the normalization of the  $\log(N) - \log(S)$ . We expect between 23 and 69 spurious detections due to statistical fluctuations (see Sect.4.2), that correspond to a percentage between  $\sim 11$  and  $\sim 33$  % in the sample of the  $\sim 208$  unidentified sources. This means that 2-5 unidentified sources among those used in the fit of the  $\log(N) - \log(S)$  could be spurious. We have checked that their contribution does not introduce any significant systematics in the best fit values.

The integrated flux is  $\sim 4.5 \times 10^{-13} \text{ erg cm}^{-2} \text{ s}^{-1} \text{ deg}^{-2}$  corresponding to  $\sim 1.4\%$  of the intensity of the X-ray background in the 14–170 keV energy band as measured by HEAO-1 (Gruber et al. 1999).

We have compared this  $\log(N) - \log(S)$  law with the one derived from the *INTEGRAL* data (Krivonos et al. 2007) in the 17 – 60 keV band. To convert our  $\log(N) - \log(S)$  into the 17 – 60 keV band we use the Crab spectral parameters derived by the *INTEGRAL* analysis (Laurent et al. 2003). We find a slope of  $\alpha = 1.62 \pm 0.08$  and a normalization of  $240 \pm 12$  sources with flux higher than 1 mCrab, corresponding to a density of  $(5.8 \pm 0.3) \times 10^{-3} \text{ deg}^{-2}$ . These parameters are in full agreement with those reported by Krivonos et al. (2007).

## 7. Conclusions

We have analyzed the BAT hard X-ray survey data of the first 39 months of the *Swift* mission. To this purpose we developed a dedicated software (Segreto et al. 2009) that performs data reduction, background subtraction, mosaicking and source detection on the BAT survey data. This software is completely

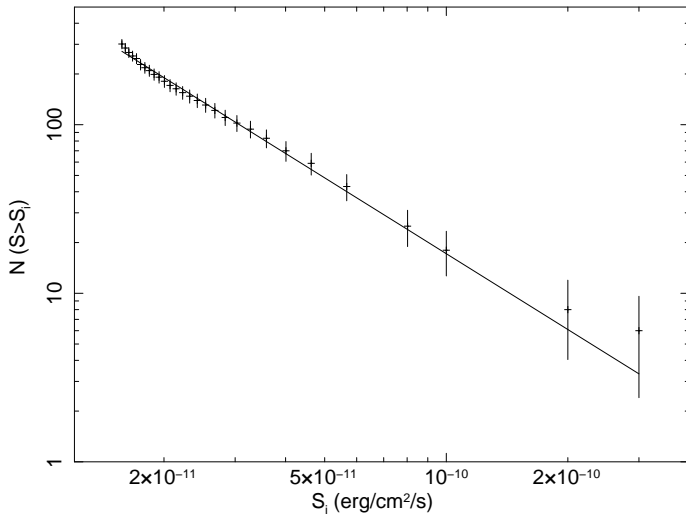


**Fig. 11.**  $\log(N)$ - $\log(S)$  distribution for the BAT extragalactic sources.

independent from the one developed by the *Swift*-BAT team. It is a single tool that provides all the products relevant to the BAT survey sources (e.g. images, spectra, lightcurves).

The large BAT field of view, the large geometrical area, and the *Swift* pointing strategy have allowed to obtain an unprecedented, very sensitive and quite uniform sky coverage that has provided a significant increase of sources detected in the hard X-ray sky. The survey flux limit is  $2.5 \times 10^{-11} \text{ erg cm}^{-2} \text{ s}^{-1}$  (1.1 mCrab) for 90% of the sky and  $1.8 \times 10^{-11} \text{ erg cm}^{-2} \text{ s}^{-1}$  (0.8 mCrab) for 50% of the sky.

We have derived a catalogue of 754 identified sources detected above a significance threshold of 4.8 standard deviations. The association of these sources with their counterparts has been performed in three alternative strategies: cross-correlation with the INTEGRAL General Reference Catalogue and with previously published BAT catalogues (Markwardt et al. 2005; Tueller et al. 2008; Ajello et al. 2008a); analysis of soft X-ray field observations with *Swift*-XRT, *XMM-Newton*, *Chandra*, *BeppoSAX*; cross-correlation with the SIMBAD catalogues of Seyfert Galaxies, QSOs, LINERs, Blazars, Cataclysmic Variables, X-ray binaries. The expected total number of spurious identifications is negligible. A set of 208 detections are not associated with a counterpart, yet. These candidate sources will be object of a follow-up campaign with *Swift*-XRT in the immediate future.

The extragalactic sources represents  $\sim 69\%$  of our catalogue (519 objects),  $\sim 27\%$  are Galactic objects,  $\sim 4\%$  are already known X-ray or gamma ray emitters whose nature is still to be determined. Compared with the 3rd ISGRI catalogue (Bird et al. 2007), we identify 176 more Seyfert galaxies, 26 more normal galaxies, 13 more galaxy clusters, 13 more QSO, 57 more Blazars and 5 more LINERs. The redshift limit for the detected emission line AGNs is  $\sim 0.4$ , with 31 objects with  $z > 0.1$ . Blazars and QSOs are detected up to  $z \sim 3.7$  and  $z \sim 2.4$ , respectively. Among the Galactic sources we significantly increase the number of cataclysmic variables detected in the hard X-ray band (29 new objects). We also detect 22 X-ray binaries that are not included in the ISGRI catalogue, even

though the total number of X-ray binaries we detect is lower than the sample included in the ISGRI catalogue.

Based on the extragalactic sources sample and on the achieved sky coverage, we have evaluated the  $\log(N) - \log(S)$  distribution for fluxes higher than  $1.5 \times 10^{-11} \text{ erg cm}^{-2} \text{ s}^{-1}$ . The slope  $1.55 \pm 0.06$  is consistent with an Euclidean distribution. We estimate that the total number of extragalactic sources at  $|b| > 5^\circ$  and flux greater than  $1.0 \times 10^{-11} \text{ erg cm}^{-2} \text{ s}^{-1}$  is  $\sim 566$ . Converting this  $\log(N) - \log(S)$  into the 17–60 keV band, our results are in full agreement with those reported by Krivonos et al. (2007) for the INTEGRAL survey. The integrated flux of this extragalactic sample is  $\sim 1.4\%$  of the Cosmic X-ray background in the 14–150 keV range (Gruber et al. 1999; Churazov et al. 2007; Frontera et al. 2007; Ajello et al. 2008c).

Forthcoming papers will be focussed on the detection of transient sources, spectral properties of the extragalactic sample, updates of the catalogue.

*Acknowledgements.* G. C. acknowledges B. Sacco and M. Ajello for useful discussions that helped to improve this paper. This research has made use of NASA’s Astrophysics Data System Bibliographic Services, of the SIMBAD database, operated at CDS, Strasbourg, France, as well as of the NASA/IPAC Extragalactic Database (NED), which is operated by the Jet Propulsion Laboratory, California Institute of Technology, under contract with the National Aeronautics and Space Administration. This work was supported by contract ASI/INAF I/011/07/0.

## References

- Ajello, M., Greiner, J., Kanbach, G., Rau, A., Strong, A. W., & Kennea, J. A. 2008a, *ApJ*, 678, 102  
 Ajello, M., et al. 2008b, *ApJ*, 673, 96  
 Ajello, M., et al. 2008c, *ApJ*, 689, 666  
 Barthelmy, S. D., et al. 2005, *Space Science Reviews*, 120, 143  
 Bassani, L., et al. 2006, *ApJ*, 636, L65  
 Beckmann, V., Soldi, S., Shrader, C. R., Gehrels, N., & Produit, N. 2006, *ApJ*, 652, 126  
 Bird, A. J., et al. 2007, *ApJS*, 170, 175  
 Bird, A. J., et al. 2006, *ApJ*, 636, 765  
 Bird, A. J., et al. 2004, *ApJ*, 607, L33  
 Brandt, W. N., & Hasinger, G. 2005, *ARA&A*, 43, 827  
 Cappelluti, N., et al. 2007, *ApJS*, 172, 341  
 Churazov, E., et al. 2007, *A&A*, 467, 529  
 Cordier, B., et al. 1991, *Advances in Space Research*, 11, 169  
 Fenimore E. E & Cannon T. M. 1978, *Appl. Opt.* 17, 337  
 Forman, W., Jones, C., Cominsky, L., Julien, P., Murray, S., Peters, G., Tananbaum, H., & Giacconi, R. 1978, *ApJS*, 38, 357  
 Frontera, F., et al. 2007, *ApJ*, 666, 86  
 Gehrels, N., et al. 2004, *ApJ*, 611, 1005  
 Górski, K. M., Hivon, E., Banday, A. J., Wandelt, B. D., Hansen, F. K., Reinecke, M., & Bartelmann, M. 2005, *ApJ*, 622, 759  
 Gruber, D. E., Matteson, J. L., Peterson, L. E., & Jung, G. V. 1999, *ApJ*, 520, 124  
 Huchra, J., & Sargent, W. L. W. 1973, *ApJ*, 186, 433  
 Jager, R., et al. 1997, *A&AS*, 125, 557

- Kendall M. G., 1980, *Multivariate analysis*, ed. Grin & co. London
- Krivonos, R., Revnivtsev, M., Lutovinov, A., Sazonov, S., Churazov, E., & Sunyaev, R. 2007, *A&A*, 475, 775
- Krivonos, R., Vikhlinin, A., Churazov, E., Lutovinov, A., Molkov, S., & Sunyaev, R. 2005, *ApJ*, 625, 89
- Laurent, P., et al. 2003, *A&A*, 411, L185
- Lebrun, F., et al. 2003, *A&A*, 411, L141
- Markwardt, C. B., Tueller, J., Skinner, G. K., Gehrels, N., Barthelmy, S. D., & Mushotzky, R. F. 2005, *ApJ*, 633, L77
- Moretti, A., Campana, S., Lazzati, D., & Tagliaferri, G. 2003, *ApJ*, 588, 696
- Pavlinisky, M. N., Grebenev, S. A., & Sunyaev, R. A. 1994, *ApJ*, 425, 110
- Pavlinisky, M. N., Grebenev, S. A., & Sunyaev, R. A. 1992, *Soviet Astronomy Letters*, 18, 116
- Sazonov, S., Revnivtsev, M., Krivonos, R., Churazov, E., & Sunyaev, R. 2007, *A&A*, 462, 57
- Schmidt, M. 1968, *ApJ*, 151, 393
- Segreto A. et al. 2009, *A&A*, submitted
- Skinner, G. K., Ponman, T. J., Hammersley, A. P., & Eyles, C. J. 1987, *Ap&SS*, 136, 337
- Skinner, G. K., Willmore, A. P., Eyles, C. J., Bertram, D., & Church, M. J. 1987, *Nature*, 330, 544
- Sunyaev, R. A., et al. 1991, *Advances in Space Research*, 11, 177
- Tueller, J., Mushotzky, R. F., Barthelmy, S., Cannizzo, J. K., Gehrels, N., Markwardt, C. B., Skinner, G. K., & Winter, L. M. 2008, *ApJ*, 681, 113
- Tully, R.B., *Nearby Galaxies Catalogue (NBG)*, 1988, Cambridge University Press
- Ubertini, P., et al. 2003, *A&A*, 411, L131
- Ubertini, P., Bazzano, A., Cocchi, M., Heise, J., in't Zand, J. J. M., Muller, J. M., Natalucci, L., & Smith, M. J. S. 1999, *Astrophysical Letters Communications*, 38, 301
- Winkler, C., et al. 2003, *A&A*, 411, L1
- Wood, K. S., et al. 1984, *ApJS*, 56, 507
- Worsley, M. A., Fabian, A. C., Bauer, F. E., Alexander, D. M., Brandt, W. N., & Lehmer, B. D. 2006, *MNRAS*, 368, 1735
- Worsley, M. A., et al. 2005, *MNRAS*, 357, 1281
- Zdziarski, A. A., Poutanen, J., & Johnson, W. N. 2000, *ApJ*, 542, 703



























Table 2: continued.

PBC name	ID	Type*	RA (deg)	Dec (deg)	Error radius (arcmin)	Offset (arcmin)	SNR	Flux <sup>†</sup> (erg cm <sup>-2</sup> s <sup>-1</sup> )	Hardness ratio (R <sub>30-150</sub> /R <sub>14-30</sub> )	Redshift	log L <sub>14-150</sub> (erg s <sup>-1</sup> )	Flag <sup>‡</sup> A B C D E	
720	PBC J2229.4+6647	IGR J22292+6647	AGN	337.36761	66.79736	3.94	1.786	7.43	1.46 ± 0.20	...	...	3 1 y h a	
721	PBC J2229.6-0831	PKS 2227-08	BLA	337.42233	-8.51841	4.09	1.830	4.98	0.94 ± 0.20	...	1.5615	47.27	1 1 n h c
722	PBC J2232.4+1144	4C +11.69	BLA	338.11536	11.73350	3.01	2.141	7.91	1.47 ± 0.19	1.14 ± 0.48	1.0370	47.02	1 1 n h a
723	PBC J2234.8-2541	ESO 533-50	Sy2	338.70361	-25.69987	4.02	1.419	5.27	1.04 ± 0.22	...	0.0263	43.22	3 1 n h b
724	PBC J2235.6-2601	NGC 7314	Sy1	338.92114	-26.03266	1.99	1.548	17.22	3.25 ± 0.23	0.77 ± 0.18	0.0047	42.22	3 1 y h a
725	PBC J2236.0+3358	NGC7319 (Stephan)	Sy2	339.00406	33.97384	2.51	0.575	10.58	1.91 ± 0.19	1.05 ± 0.34	0.0221	43.43	3 1 y h a
726	PBC J2236.7-1232	Mrk 915	Sy1	339.19135	-12.54211	2.72	0.231	13.46	3.01 ± 0.22	1.36 ± 0.32	0.0240	43.48	1 1 y h a
727	PBC J2240.2+0802	RHS 59	Sy1	340.05978	8.04542	3.33	0.832	6.76	1.23 ± 0.20	1.14 ± 0.59	0.0250	43.34	1 1 n h b
728	PBC J2245.8+3939	3C 452	Sy2	341.45032	39.66523	2.61	1.350	13.37	2.91 ± 0.22	1.56 ± 0.34	0.0810	44.55	1 1 y h a
729	PBC J2251.8+2215	87GB 224928.1+220114	BLA	342.97150	22.26663	4.03	1.626	5.71	0.97 ± 0.19	...	3.6680	48.11	3 1 n h c
730	PBC J2253.9+1609	3C 454.3	BLA	343.48819	16.16178	1.36	0.826	41.15	8.30 ± 0.20	1.45 ± 0.10	0.8590	47.44	1 1 y h a
731	PBC J2254.0-1734	RBS 1913	Sy1	343.52182	-17.57691	1.41	0.343	30.01	5.55 ± 0.19	0.88 ± 0.10	0.0639	44.84	3 1 y h a
732	PBC J2254.3+1146	MCG+02-58-032	Sy2	343.58633	11.78212	4.08	0.255	8.47	1.59 ± 0.21	...	0.0285	43.38	1 1 n h b
733	PBC J2255.3-0310	AO Psc	DQ*	343.82910	-3.18121	1.89	0.312	20.41	2.86 ± 0.23	< 0.03	...	...	2 1 n h c
734	PBC J2258.9+4055	MCG +07 -47 -002	Sy1	344.73630	40.92973	3.22	0.253	7.78	1.60 ± 0.21	0.98 ± 0.40	0.0171	43.04	1 1 n h c
735	PBC J2259.6+2454	RBS 1922	Sy1	344.91025	24.90242	2.74	1.573	9.17	1.63 ± 0.19	0.77 ± 0.31	0.0338	43.73	3 1 n h c
736	PBC J2302.1+1558	NGC 7465	LIN	345.53625	15.98235	4.03	2.109	9.05	1.68 ± 0.20	...	0.0065	42.06	1 1 n h b
737	PBC J2303.3+0852	NGC 7469	Sy1	345.82596	8.87315	1.67	0.615	28.28	5.77 ± 0.21	0.94 ± 0.11	0.0158	43.43	3 1 y h a
738	PBC J2304.7-0841	Mrk 926	Sy1	346.18387	-8.68914	1.28	0.261	36.74	6.11 ± 0.17	0.89 ± 0.08	0.0471	44.60	1 1 y h a
739	PBC J2304.8+1217	NGC 7479	Sy2	346.20084	12.29863	4.30	2.526	4.63	0.79 ± 0.18	...	0.0079	42.04	3 1 n h c
740	PBC J2307.2+0433	RBS 1944	Sy1	346.82056	4.55890	3.58	3.548	6.08	0.88 ± 0.18	0.78 ± 0.58	0.0420	43.66	3 1 n h c
741	PBC J2318.3-4221	NGC 7582	Sy2	349.59927	-42.36063	1.52	0.600	31.07	5.56 ± 0.19	0.92 ± 0.10	0.0052	42.49	3 1 n h a
742	PBC J2318.9+0014	Mrk 530	Sy1	349.72592	0.24491	2.11	0.603	14.09	2.46 ± 0.18	0.92 ± 0.22	0.0292	43.78	3 1 y h a
743	PBC J2319.6+2616	RX J2319.5+261	CV*	349.90530	26.27489	3.52	1.852	7.04	1.24 ± 0.21	0.56 ± 0.35	...	...	3 1 n h c
744	PBC J2323.3+5849	Cas A	SNR	350.84976	58.82223	1.33	0.813	41.18	7.52 ± 0.20	0.31 ± 0.04	...	...	2 1 y l a
745	PBC J2325.4-3827	RBS 2004	Sy1	351.36133	-38.46166	3.84	1.004	5.46	0.88 ± 0.17	0.54 ± 0.44	0.0358	43.52	3 1 n h c
746	PBC J2325.8+2152	RHS 61	Sy1	351.46313	21.88039	3.40	0.962	9.16	1.79 ± 0.21	0.84 ± 0.32	0.1200	44.74	1 1 n h a
747	PBC J2327.4+0939	PKS J2327+0940	BLA	351.86725	9.65903	3.47	1.476	9.60	1.99 ± 0.21	...	1.8430	47.55	1 1 n h c
748	PBC J2329.0+0329	NGC 7682	Sy2	352.25446	3.49787	3.71	2.252	5.64	1.21 ± 0.24	...	0.0170	42.97	1 1 n h c
749	PBC J2331.0+7123	IGR J23308+7120	Sy2	352.75507	71.38662	3.32	3.236	6.81	1.11 ± 0.19	0.80 ± 0.46	0.0370	43.53	3 1 y h a
750	PBC J2333.9-2343	RBS 2022	Sy?	353.47760	-23.72896	4.12	0.153	4.92	0.71 ± 0.17	...	0.0478	43.58	1 0 n h b
751	PBC J2341.9+3036	MCG+05-55-047	G	355.47964	30.61338	3.19	1.884	8.57	1.51 ± 0.20	1.03 ± 0.42	0.0174	43.02	3 1 n h c
752	PBC J2351.7-0109	4C -01.61	Sy1	357.94022	-1.15795	3.83	2.629	7.33	1.52 ± 0.22	...	0.1740	44.99	1 1 n h b
753	PBC J2359.1-6055	2MASX J23590436-6054594	Sy2	359.78470	-60.92285	4.40	0.617	5.79	0.95 ± 0.20	...	0.1014	44.36	2 3 n h b
754	PBC J2359.1-3035	H 2356-309	BLA	359.79602	-30.58918	4.08	2.385	5.00	0.58 ± 0.12	...	0.1671	44.90	3 3 n h b

\* The source type is coded according to the nomenclature used in SIMBAD.

† Flux is in units of 10<sup>-11</sup> erg cm<sup>-2</sup> s<sup>-1</sup>.‡ Flag A: energy band with highest significance (1=14–150 keV; 2=14–30 keV; 3= 14–70 keV);  
Flag B: energy band used for the calculation of the flux (1=14–150 keV; 2=14–30 keV; 3= 14–70 keV);  
Flag C: y if already reported as hard X-ray source;  
Flag D: l if the source has |b| < 5°, h if the source has |b| > 5°;  
Flag E: strategy used for the identification (see Sect.4.3);